Electrochemical leaching of rare-earth elements from spent NdFeB magnets

Makarova Irina, Soboleva Ekaterina, Osipenko Maria, Kurilo Irina, Laatikainen Markku, Repo Eveliina

DOI: 10.1016/j.hydromet.2020.105264

Electrochemical Leaching of Rare-Earth Elements from Spent NdFeB Magnets

Irina Makarova[1,], Ekaterina Soboleva[2], Maria Osipenko[3], Irina Kurilo[4], Markku Laatikainen[1], Eveliina Repo[1]*

[1] Department of Separation and Purification Technology, School of Engineering Science, LUT University, Skinnarilankatu 34, FI-53850, Finland

[2] Department of Physics, School of Engineering Science, LUT University, Skinnarilankatu 34, FI-53850, Finland

[3] Department of Chemistry, Technology of Electrochemical Production and Electronic Engineering Materials, Belarussian State Technological University, Sverdlova 13a str, 220050, Minsk, Republic of Belarus

[4] Department of Analytical and Physical Chemistry, Belarussian State Technological University, Sverdlova 13a str, 220050, Minsk, Republic of Belarus

Abstract

Spent NdFeB magnets are highly appealing secondary resources for rare earth elements (REEs), especially for Nd. The goal of this study was to investigate electrochemical leaching of Fe and rare earths from NdFeB magnets with sulfuric and oxalic acids at different acid concentrations and current densities and reveal the mechanism of the leaching in varying conditions. The metals were leached from polished magnet surface and from crushed magnets using a 3D-printed Ti basket. Electron and atomic force microscopic analysis showed a highly heterogeneous structure of the magnets containing on average 60 wt-% of Fe and 25 wt-% of Nd. According to Kelvin probe force microscopy, the Volta potential difference between the matrix and the REE-rich grains was over 500 mV. Addition of oxalic acid ($H_2C_2O_4$) in the sulfuric acid leach solution allows leaching at lower cell voltage and separation of the REE-oxalate precipitates. Some incorporation of rare-earth element oxalates in the cathodic sediment was also observed. Finally, the leaching mechanism is discussed.

Keywords: Leaching; Electrolysis; Rare earth elements; spent NdFeB magnet

1. Introduction

The demand for rare-earth elements (REEs) is nowadays higher than the supply and the prices of these metals are expected to increase in the near future. Especially, concerns are arising due to a monopoly and strong export quota on rare earths of China and scarcity of rare-earth ores in Europe. While new alternative materials do not exist, the most effective way to solve the problem is developing an affordable recycling technology [1, 2].

Fluorescent lamps [3, 4] and permanent magnets are typical secondary resources of REEs, The last ones are widely used in electromechanical, magnetomechanical, and electronic applications [5, 6]. Currently, the strongest permanent magnet is a neodymium magnet (also

known as NdFeB, NIB, or Neo magnet). This type of rare-earth magnet is made from an alloy of neodymium, iron, and boron to form the $Nd_2Fe_{14}B$ tetragonal crystalline structure. The magnetic properties, as well as corrosion resistance strongly depend on the alloy composition, microstructure and manufacturing technique employed [7]. Also, various dopants are used to improve the properties of the magnets. Two types of NdFeB dopants have been mentioned in the literature [8−15]. Type (1) dopants are Al [8, 9], Ga [10], Cu [11, 12], Co [13], Ge, Sn and Zn, and type (2) dopants are V [14], Mo [15], W [15], Nb [15] and Ti. Both types of dopants influence on the microstructure in a different way and increase the magnetic coercivity or improve the corrosion resistance of the magnet. According to Schultz et al. [16], however, the alloy modifications improve corrosion resistance only to a certain degree. Another way is to coat the magnet with Al [17], Zn or Ni-Cu. These metals are important, because they influence on the recycling technology and purity of the final product.

High concentration of Nd and Dy in the NdFeB magnets makes them an important material for recycling. Many different technologies for REEs recovery have been proposed [18−37]. Among them are chlorination [18], hydrogen decrepitation and direct reuse [19], selective leaching or precipitation [20−24], glass slag methods [25], solvent extraction [26−31], electrolysis in molten salts [32−34], gas phase extractions [35], and bioleaching [36]. The aim of all these methods is to maximize selectivity, which is, however, a difficult task due to similarity of REEs. Furthermore, they have many disadvantages such as high cost, high energy consumption for heating, and difficult utilization of the waste. Among the studied methods, the simplest way to separate REEs from other metals includes leaching and chemical precipitation. Hoogerstraete et al. [1] showed that it is possible to use oxalic acid, which is a strong complexing agent for Nd, in the leaching process to form precipitates (solubility product of $Nd_2(C_2O_4)_3$ is $1.08 \cdot 10^{-33}$) [37]. Another possible variant is to add an alkali to obtain mixed double sulfate salts [6, 25]. At the same time Ambikadevi and Lalithambika [38] concluded that oxalic acid is also the most efficient for dissolving iron oxides, so it is possible to use mixture of mineral and oxalic acids in order to reach a better leaching efficiency.

Besides conventional acid leaching, Parkash et al. [39−41] have demonstrated several electrochemical technologies in which REEs have been selectively and efficiently extracted at room temperature. These methods include a dual anode strategy [39] and using two-[40] and three-[41] chambered membrane reactors enabling highly efficient and eco-friendly possibility for REE recycling. However, it is necessary to note that REEs are highly reactive elements and

cannot be recovered from the aqueous solutions directly on the cathode [42], but instead electrochemistry can be used for anode dissolution process as shown earlier [43−45]. As an alternative route, it is quite useful to have special holders (baskets), which allow the utilization of big amount of different kind of waste and without necessity for pressing or adding electrical connections. Besides, ratio of surfaces between cathode and anode can be changed if needed and respectively it will influence on the speed of dissolution. Moreover, during electrolysis, it is possible to add waste from the top of the basket without interrupting the process. It has also been discovered recently that materials like NdFeB waste [46], for of which the principal anode reaction is oxygen evolution may continue to function as anodes when placed in a titanium basket.

However, it is vitally important to find connection between the mechanism of NdFeB alloy dissolution and possibility for direct recovery of REEs. In this study, dissolution of NdFeB magnets were investigated both with chemical and electrochemical leaching. Moreover, the alloy was extensively characterized before and after leaching using electron (SEM, EDX) and atomic force microscopy as well as chemical analyses. We were able to show effectiveness of electrochemistry-aided leaching and the underlying mechanisms were also explored. The novelty of our approach in linking understanding of the magnet composition to the leaching behavior. Furthermore, electro-leaching of the polished surfaces was extended to a more realistic system, where crushed magnets are leached in a specially designed holder.

2. Experimental

2.1 Materials

Spent NdFeB magnets from Webcraft GmbH (Germany) with the diameter of 35 mm and thickness of 5 mm were used in all experiments. The samples were demagnetized at the Curie temperature of 310 °C for 1 hour in an Entech muffle furnace. For proper demagnetization of the working area, the samples were connected by edges. In electrochemical studies NdFeB magnet was used as the anode and copper plate as the cathode (0.2 dm^2). Anodes were mechanically polished with #500, #900, #1200 and #2000 emery paper, then with Al_2O_3 suspension, and finally degreased with ethanol. Electrolysis was carried out in a galvanostatic mode of PS 3005 power supply. For some experiments, the magnet was crushed into small pieces, first with a hammer and then set between two aluminum metal plates by applying a

force of 10 tons with a hydraulic press. NdFeB magnets are brittle and break quite easily into smaller pieces (100-1000 μm).

In order to determine the total elemental composition, 0.1 g of the NdFeB magnet was dissolved in a mixture of nitric and hydrochloric acids (volume ratio HNO_3:HCl = 1:4) using Milestone Ultrawave microwave digestion system. The mixture was then filtered through 0.45 μm polypropylene filters (VWR). Three blank samples containing only acids were treated similarly and used as background.

Sulfuric acid was used as a leaching agent and it was prepared by diluting concentrated acid (Sigma-Aldrich, 98%) with MilliQ water (Merck Millipore Q-POD) to a desired concentration. Oxalic acid (Sigma-Aldrich, >97.5%) was used as a strong complexing agent for the REE ions.

2.2 Methods

All leaching experiments were carried out at 22 ± 1°C in a 150 mL glass beaker. In the electrochemical leaching experiments with the polished magnets, current densities of 10, 20 and 50 A/dm^2 were used. In some experiments, the magnet was crushed and a 3D-printed titanium basket was used as a holder (Fig. 1). In this case 0.5 M H_2SO_4 and current density of 10 A/dm^2 was used. Height of basket was 15 mm, diameter 30 mm, and size of the holes 0.05 mm. The temperature of the electrolyte was controlled by a water bath (RK8 CS, Lauda). The pH and conductivity of the leach solutions was monitored using standard procedures (Radiometer PHM 240 pH/ion pH meter and Knick 703 conductivity meter).

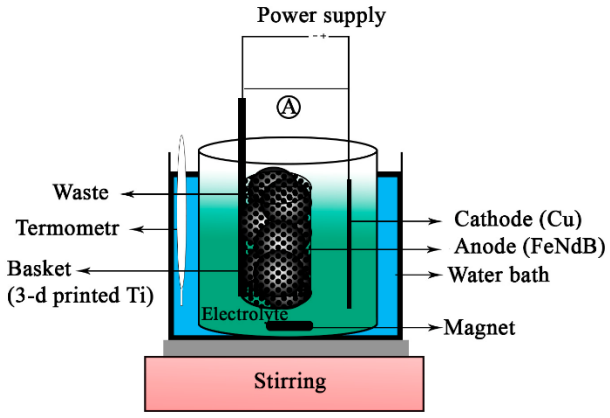

Figure 1. Schematic picture of electro-leaching in a Ti basket.

In order to choose the optimal leaching conditions, the concentration of sulfuric acid was varied between 0.05 and 0.5 mol/L. Concentration of oxalic acid in all experiments was 0.05 mol/L. Solid to liquid ratio was kept at 0.05 dm^2 of NdFeB alloy surface per 80 mL of solution and magnetic stirring speed was 400 rpm. The samples were leached for 1 h. The magnet samples were weighted before and after leaching using Mettler AC 88 analytical scale. The solution sample leachates taken during leaching were diluted with a mixture of 1% HNO_3 and 1% HCl (Ultrapure, Merck), and the metal concentrations were measured using inductively coupled plasma mass spectroscopy (ICP-MS, Agilent 7900). Relative standard deviation of all ICP measurements were less than 3.6%.

Potentiodynamic polarization scans were performed using a potentiostat-galvanostat (Autolab PGSTAT 302N, Methrom) in a three-electrode glass cell. Polarization curves were recorded at a potential sweep rate of 1 mV/s from the open circuit potential (OCP) until 1 V. The NdFeB magnet was used as the working electrode, while Pt and a saturated Ag/AgCl were used as the counter and reference electrodes, respectively. The potentials reported in the text were recalculated to the standard hydrogen electrode (SHE) scale.

The morphologies of the leached magnet surfaces and electrodeposited coatings were imaged using Hitachi SU3500 scanning electron microscopy (SEM). Elemental composition was measured by energy dispersive X-ray spectroscopy (EDX, Thermo Scientific UltraDry SDD). Precipitates obtained after dissolution in mixture of sulfuric and oxalic acids were washed thoroughly with water, digested and analyzed with ICP-MS. The chemical composition and crystal structure of the NdFeB magnet before and after leaching was further ascertained using X-ray diffraction (XRD) (Bruker D8 Advance) with Cu Kα irradiation. The 2Θ range was 10 –70° and step size 0.02 °/s.

For the optimization of electrodeposition conditions, current efficiency (ε) was calculated. In some cases, ε was more than 100% due to the active dissolution and substantial contribution of chemical process. Energy consumption W (in kWh/kg) was calculated from Eq. (1)

$$W = \frac{E}{q_{alloy}\varepsilon} \qquad (1)$$

where E is the average cell voltage on cell (V). Considering only the major components Fe and Nd, the electrochemical equivalent of the alloy q_{alloy} (in g/Ah) was calculated from Eq. (2).

$$q_{alloy} = \frac{q_{Fe} q_{Nd}}{q_{Fe} w_{Fe} + q_{Nd} w_{Nd}} \quad (2)$$

where w is the weight fraction. For iron, $q_{Fe} = M_{Fe}/z_{Fe}F = 1.05$ g/(Ah) and for neodymium $q_{Nd} = 1.79$ g/(Ah), where z is the charge of the product ion and F the Faraday constant.

The scanning Kelvin probe force microscopy (SKPFM) technique of the polished magnet samples was used to determine the local Volta potentials of the microstructure and relative nobility of the REE-rich regions. Volta potential mappings were carried out in air using atomic force microscope (MultiMode 8, Bruker) in a double pass mode (Kelvin Probe Force Microscopy): first pass measures topography (height) and second pass the local potential difference in lift mode. The mapped area (40×40 µm) was scanned with Bruker SCM-PIT probe with spring constant of ~2.8 N/m, resonant frequency of ~75 kHz and tip radius of ~20 nm. The tip speed was 8 µm/s, image resolution 512×512 pixels, and tip lift height 50 nm. AFM data was analyzed using Nanoscope Analysis V1.8 software. The first order plane fit and zeroth-order flattening were used to process the height maps. The potential maps were neither flattened nor was any filter applied to smooth the data.

All the experiments were done in triplicate to ensure statistical reliability of the results.

3. Results and discussion

The studied system is composed of highly heterogeneous solid phase in contact with a solution, where number of dissociation, complexation and precipitation equilibria are present. The composition of the polished magnet surface is first discussed in Section 3.1. Section 3.2 deals with dissolution of the metals with/without electric current and in view of the complex solution chemistry. Electro-leaching of crushed magnet is finally discussed in Section 3.3.

3.1 Characterization of the polished NdFeB magnet

Microscopic examination of the polished NdFeB magnet (Figure 2) shows the heterogeneous structure. Moreover, the matrix of the alloy is fragile and part of the grains ranging from 2 to 15 μm loosens during the polishing were crumbled. Chemical composition of the different domains was analyzed using EDX mapping and the results for the major components is shown in Fig. 2. The compositions at specific locations A, B, and C are listed in Table 1. The maps for the minor additives are given in Fig. 1S in the supplementary material.

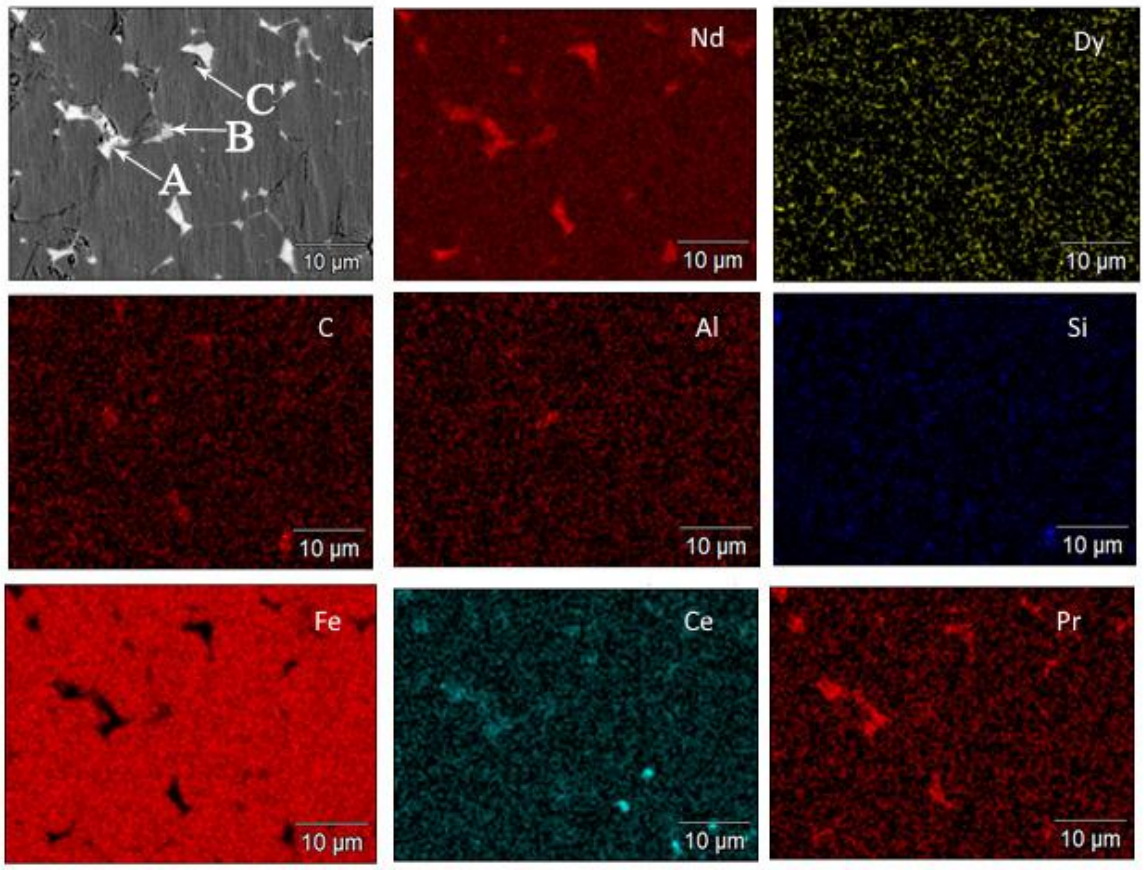

Fig. 2. High-resolution EDX mapping of the main elements on the spent NdFeB magnet surface showing different chemical composition.

Table 1. Composition of domains A-C in Figure 1 determined by EDX.

Element	A (light grain)		B (bright grain)		C (dark grain)	
	wt-%	mol-%	wt-%	mol-%	wt-%	mol-%
C	7.3		3.9		2.2	
O	0.8		1.3			
Al	0.3		0.5		0.6	
Si	1.4		–		–	
P	0.6		–		–	
Fe	10.2	12.3	10.3	18.1	67.6	74.6

Ce	10.2		14.6		4.8	
Pr	15.6		21.1		5.1	
Nd	53.8	25.3	48.3	33.1	18.7	8.0
Gd	−		−		0.6	
Dy	−		−		0.3	
Fe : Nd		1 : 2		1 : 1.8		9.3 : 1

The maps clearly show that Fe is most abundant in the matrix, while Nd and Pr are located in the grains and concentrated on the grain boundaries. Dy and Ce are nearly evenly distributed over the surface. Boron was not analyzed. It should be noticed that carbon, which is evenly spread in this alloy, inhibits the leaching process [47] because the surface becomes covered with a black slime of graphite. Other impurities (e.g. Ca, C1, O and Pr), however, are considered as a starting point of the leaching [47]. Dy and Nb, on the other hand, have an opposite influence as the increase of their concentration enhances the corrosion resistance of NdFeB inhibiting its dissolution [48]

According to Table 1 and Fig. 1S, the ferromagnetic matrix consists mainly of Nd and Fe with a mole ratio of 1.5-2/14 and thus represents the ϕ-phase ($Nd_2Fe_{14}B$) [16]. The grains rich in Nd, Pr and Ce have a mole ratio of Nd and Fe around 2/1, which is substantially lower than the value 4 /1 reported for the Nd-rich n-phase [16].

The Volta potential indicates the relative tendency of metals for oxidation and can help to assess the severity of localized dissolution in the systems with complex microstructures [49−51]. In a galvanic couple, the phase with higher electrochemical nobility has typically higher Volta potential and usually acts as a cathode, whereas that with lower Volta potential acts as an anode. SKPFM mapping revealed sub-micron or nanometer-sized structure of the alloy, as seen in Figure 3. The potential difference between $Nd_2Fe_{14}B$ ϕ-phase and the Nd-rich anodic phases varied up to 500 mV, which usually is sufficient to initiate selective dissolution of such anodic sites. The potential difference averaged over the whole surface was 213 mV ± 50 mV. The ratio of the sizes between different phases is one of the main parameters effecting on in the leaching process (larger size of the cathodic phase enhances leaching due to enhanced oxygen reduction) [52].

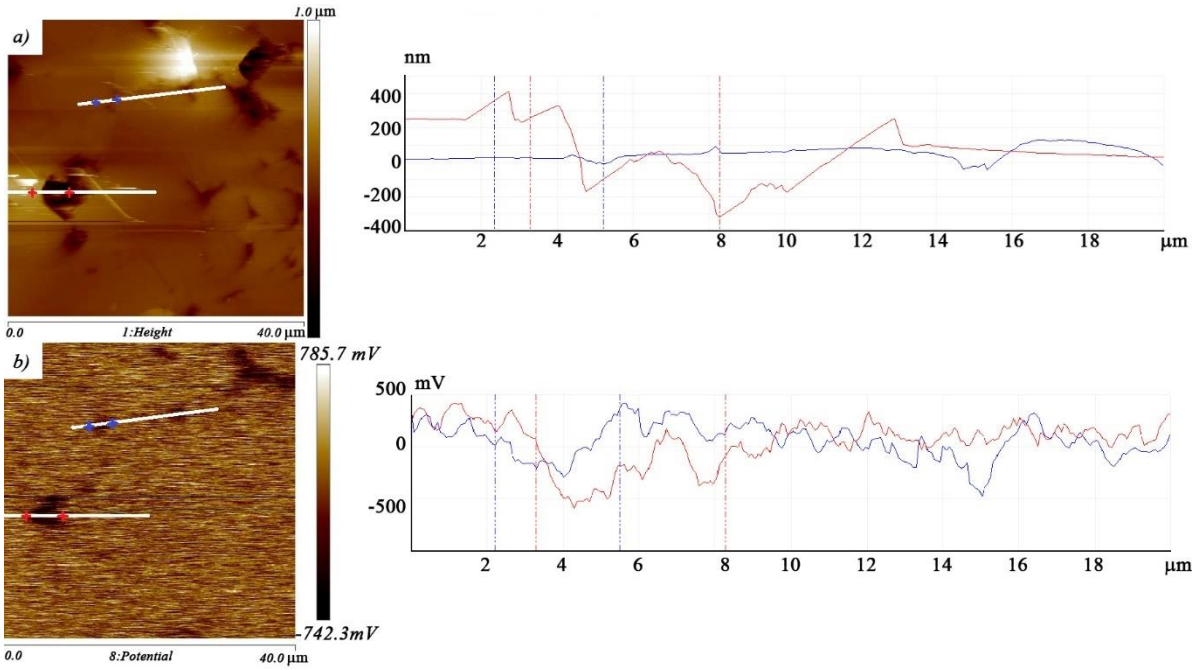

Figure 3. (a) Topography and (b) Volta-potential map measured using SKPFM in air on the surface of polished NdFeB magnet. Profile analysis in each map is a section along two lines.

In summary, EDX, SEM, and SKPFM data confirmed the presence of domains with different chemical composition and high differences in local Volta potential, which both have important impact on the leaching process as discussed below.

3.2 Chemical and electrochemical leaching

The leaching experiments discussed in this Section were made on polished NdFeB magnet surface using different leach solutions and current densities. Measurements made at $i = 0$ are referred to as chemical leaching. Effect of the current density on leaching in 0.1 M H_2SO_4 (*a*) and 0.1 M H_2SO_4 + 0.05 M $H_2C_2O_4$ (*b*) is presented in Fig. 4. Concentration of dissolved iron in solution is presented as mass by multiplying of measured by ICP analysis concentration on volume of used solution to show comparable values obtained by weighing. During the leaching there was almost linear growth of the iron concentration in the solution, except for the case of the highest current density (20 A/dm^2). This is connected to a process of cation accumulation and iron electrodeposition that begins to take place at these conditions. Concentration of Fe^{2+} ions in the presence of $H_2C_2O_4$ was nearly twice as low suggesting formation of insoluble FeC_2O_4 (Fig. 4b) that may lead to surface passivation. On the other hand, it was observed that

increasing of oxalate-ions concentration to 0.1 M shows similar behavior to 0.05 M $H_2C_2O_4$ during leaching process (Fig. 3S). Consequently, during the first 30 minutes Fe dissolution was low and then increased due to activation of surface. Similar behavior of REEs in the presence of oxalic acid will be explained later.

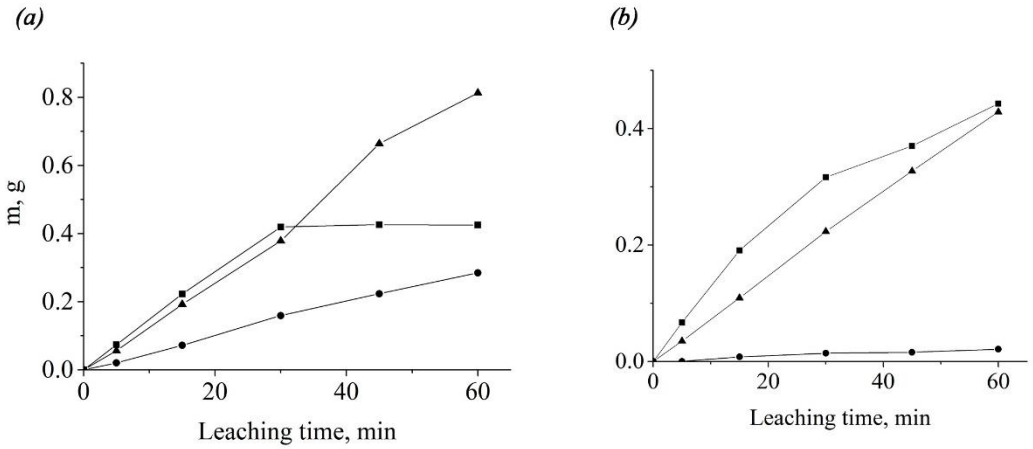

Figure 4. Effect of current density on iron leaching from NdFeB magnet waste in (*a*) 0.1 M H_2SO_4 and (*b*) 0.1 M H_2SO_4 + 0.05 M $H_2C_2O_4$. Stirring rate 400 rpm, T = 23 °C, i = 0 A/dm^2 (circles), 10 A/dm^2 (triangles), 20 A/dm^2 (squares).

Weight loss of NdFeB alloy during chemical and electrochemical leaching is listed in Table 2. It is established that a loss of alloy weight strongly depended on the composition of the electrolyte and the applied current density. Even without electricity, NdFeB was rapidly and effectively leached in 0.5 M H_2SO_4. Increasing of the current density up to 20 A/dm^2 led to a gradual increase of the weight loss but in the presence of oxalic acid even at the current density of 50 A/dm^2 the weight loss was clearly lower. This can be attributed to the passivation of the alloy surface. Moreover, there is a plateau in iron dissolution curve after 30 minutes at current density of 20 A/dm^2 in sulfuric acid leaching, but no passivation was observed at 10 A/dm^2. Inhibition of the iron dissolution at lower current densities can be explained by intensification of cathodic and anodic processes that can be accompanied by several chemical transformations. First, we assume that increasing of current density leads to passivation of the surface. On the other hand, oxygen gives possibility of changing iron state from Fe^{2+} to Fe^{3+}, and finally, significant change in bulk pH during electrolysis leads to formation of dispersed phases, like $Fe(OH)_3$, that finally precipitate.

In the presence of oxalate, the weight loss of NdFeB alloy was less at all concentrations, which is most likely due to the formation of insoluble oxalates on the NdFeB surface. It should be

noticed that the mass losses during the electrolysis differ from those calculated theoretically according to Faraday's law because of the high reactivity of the magnet and mechanical degradation of the matrix during the leaching [39].

Table. 2 Weight loss of NdFeB magnet during chemical and electrochemical leaching

	0.5 M H_2SO_4		0.1 M H_2SO_4		0.05 M H_2SO_4		Theoretical value*
	–	0.05M $H_2C_2O_4$	–	0.05M $H_2C_2O_4$	–	0.05M $H_2C_2O_4$	
i, A/dm^2	Δm, g						
Chemical leaching	1.46 ± 0.03	1.11 ± 0.13	0.45 ± 0.04	0.089 ± 0.08	0.029 ± 0.005	0.009 ± 0.002	–
10	1.64 ± 0.11	1.19 ± 0.08	0.74 ± 0.03	0.67 ± 0.07	0.61 ± 0.04	0.67 ± 0.01	0.76
20	1.68 ± 0.07	1.48 ± 0.06	1.32 ± 0.05	0.80 ± 0.07	–	–	1.51
50	2.97 ± 0.14	1.07 ± 0. 02	–	–	–	–	3.78

* $\Delta m = Iq_{alloy}t$, where I is current (A), q_{alloy} is electrochemical equivalent of the alloy, 1.51 (g/Ah) and t is time, (h).

Fig. 5 shows the leaching data for individual REEs at different current densities. Concentration of REEs increased linearly with time during chemical leaching (Fig. 5*a*) and at current density of 10 A/dm^2 (Figure 5*c*) and the leaching efficiency increased 3.5 times after applying electricity. Steady increase of REEs concentration shows that insignificant amount was included in precipitates or in the cathode deposit. However, when using current density of 20 A/dm^2, the concentration of REEs started to decrease after 30 minutes. This is probably connected to their mechanical co-deposition on the cathode (see Section 3.5 and Table 4) in the form of solid fall-down phase (it would be explained below in mechanism of leaching process, Fig. 9) or with formed oxalates (addition of $H_2C_2O_4$). Presence of $H_2C_2O_4$ strongly affected the behavior of the REEs (Figs 5*b*, 5*d* and 5*f*) which is related to the formation of oxalate complexes and precipitates (see below). After immersion of NdFeB alloy in the solution, selective leaching of most electronegative components takes place first. During the first 30 minutes of electrochemical leaching (Figs 5*d* and 5*f*), concentration of REEs remained constant while the REE/oxalate ratio corresponded to the forming of complexes. The REE complexes adsorb on the anode surface and form passive layer. Besides, it is possible that slightly soluble carbonates form due to oxidation of oxalic acid. After that, an increase of dissolved REEs was observed, but their amount in the solution was 3−20 times less than in the

leaching solution without $H_2C_2O_4$. Increasing the oxalate concentration from 0.05 to 0.1 M (Figs 5*b* and 6S) enhanced dissolution of REEs, but the behavior around 30 min activation period was similar, possibly due to formation and dissolution of oxalate species [53, 54]. The precipitate formed during electro-leaching in the presence of $H_2C_2O_4$, was analyzed with XRD and after digestion with ICP-MS (Table 3 and Figure 4S in supplementary material). The XRD profile showed formation of $Nd_2(C_2O_4)_3 \cdot 10H_2O$ powder, which is supported by the results presented in Table 3.

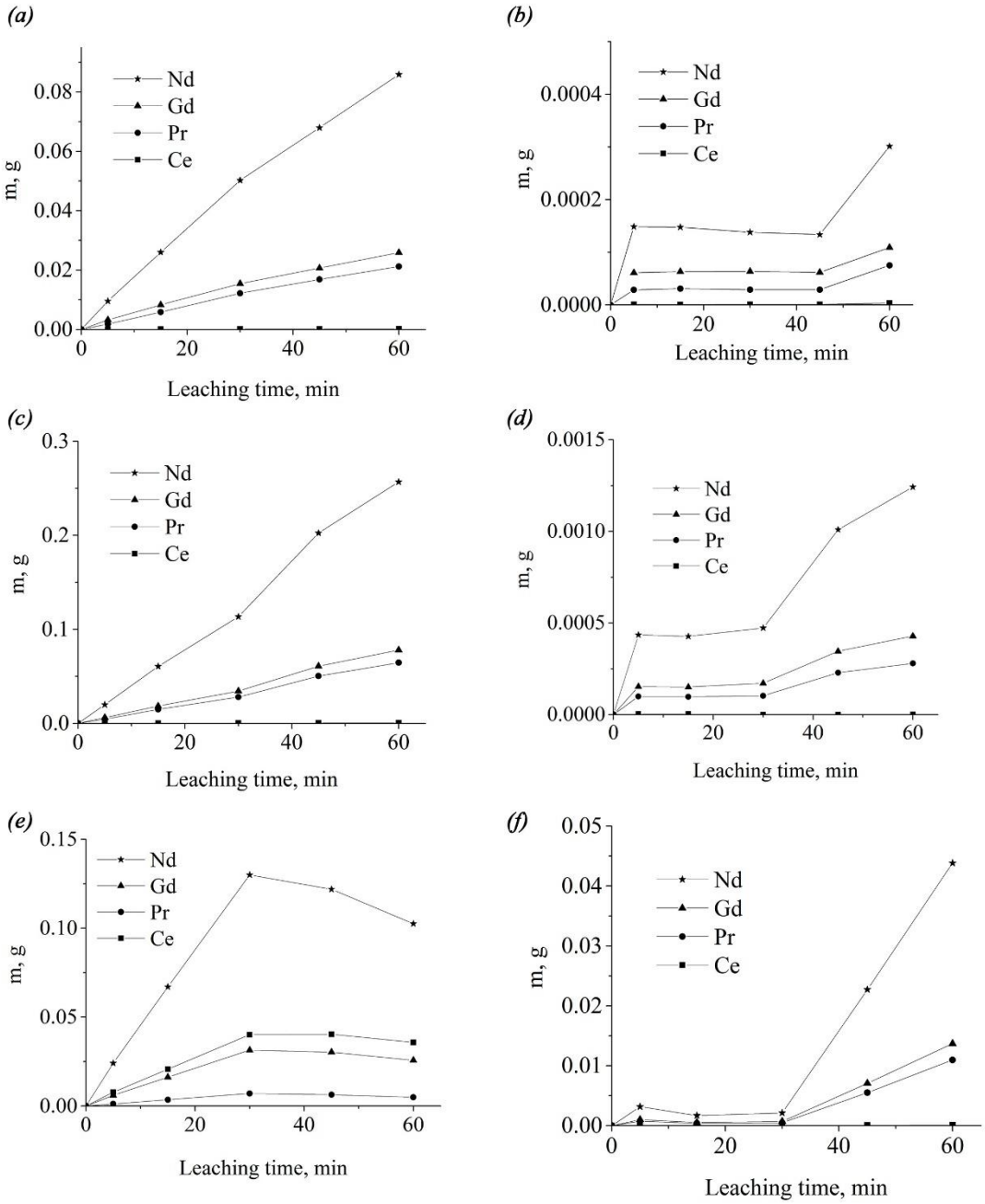

Figure 5. Effect of current density on the leached weight of REEs from NdFeB magnet waste in (*a, c, e*) 0.1 M H_2SO_4 and (*b, d, f*) 0.1 M H_2SO_4 + 0.05 M $H_2C_2O_4$; (*a, b*) chemical leaching;

electrochemical leaching at current density, (*c*, *d*) 10 A/dm^2 and (*e*, *f*) 20 A/dm^2 (Stirring rate 400 rpm, *T* = 23 °C).

Table 3. Metal composition of the precipitate after chemical and electrochemical leaching in the mixture of 0.1 M H_2SO_4 and 0.05 M $H_2C_2O_4$.

	Fe	Cu	Nd	Ce	Pr	Gd
	g/kg					
chemical leaching	2.8	0.8	295.0	0.7	87.0	75.5
10 A/dm^2	3.1	0.5	291.3	0.7	85.0	75.1
20 A/dm^2	3.1	0.5	289.7	0.7	83.4	75.0

* amount of Tb, Dy, Ho, Er, Yb, La, Sm was 0.03−0.09 g/kg

In the presence of oxalic acid (Figs 5*b*, 5*d* and 5*f*), the REEs concentration in the solution remained nearly constant for the first 30 min probably because of precipitation of the dissolved metals as oxalates (see Eq. (5*d*) below). After consumption of the oxalate, the REEs concentration started to increase. All REEs form insoluble salts with oxalate with solubility products pK_{sp} = 26 − 33 [37] and the solution concentration should be extremely low. The relatively high amount of REEs in the solution is assumed to be due to the presence of soluble oxalate complexes.

According to the leaching data, NdFeB alloy is highly reactive with sulfuric acid even without electric current. Chemical dissolution in sulfuric acid can be described by following overall reactions [55].

$$Nd_2Fe_{14}B + 17H_2SO_4 \rightleftharpoons 2Nd^{3+} + 14Fe^{2+} + 17SO_4^{2-} + 17H_2 + B \quad (3)$$

Boron is further converted into its oxide and sulfur dioxide is released as shown in Eq. (4).

$$2B + 2H_2SO_4 \rightleftharpoons B_2O_3 + 3SO_2 + 3H_2O \quad (4)$$

Dissolution in a mixture of sulfuric and oxalic acid takes place according to the same mechanism, but the dissolved metals form stable oxalate complexes and eventually precipitate as crystalline hydrates as shown for Nd in Eq. (5c). The solubility of Nd oxalate is extremely low (pK_{sp} = 33 [37]) and precipitation takes place immediately. For ferrous oxalate, pK_{sp} = 6.5

and according to speciation calculations (not shown here), most of dissolved iron remains in solution as sulfate and oxalate complexes. Eq. (5) is written in terms of oxalate anion but actually oxalic acid exists mainly as $H_2C_2O_4$ at pH below 1.2, whereas $HC_2O_4^-$ is the most predominant species at pH 2.5−3 [56].

$$Fe^{2+} + nC_2O_4^{2-} \rightleftharpoons [Fe(C_2O_4)_n]^{2-2n} \quad (5a)$$

$$Fe^{2+} + C_2O_4^{2-} + 2H_2O \rightleftharpoons Fe(C_2O_4)\cdot 2H_2O \quad (5b)$$

$$Nd^{3+} + nC_2O_4^{2-} \rightleftharpoons [Nd(C_2O_4)_n]^{3-2n} \quad (5c)$$

$$Nd^{2+} + nC_2O_4^{2-} \rightleftharpoons [Nd(C_2O_4)_n]^{2-2n} \quad (5d)$$

$$2Nd^{3+} + 3C_2O_4^{2-} + 10H_2O \rightleftharpoons Nd_2(C_2O_4)_3\cdot 10H_2O \quad (5e)$$

In electro-leaching, anodic dissolution of the NdFeB alloy takes place according to the reactions shown in Eq. (6). Electrooxidation of Nd has two following steps with sequential transfer of electrons (Eq. (6a, 6b)) with obtaining Nd^{3+}. The last one in aqueous solutions forms slightly soluble Nd_2O_3 and $Nd(OH)_3$.

$$Nd \rightleftharpoons Nd^{2+} + 2e^- \qquad E° = -2.2\ V \quad (6a)$$

$$Nd \rightleftharpoons Nd^{3+} + 3e^- \qquad E° = -2.323\ V \quad (6b)$$

$$2Nd + 3C_2O_4^{2-} + 10H_2O \rightleftharpoons Nd_2(C_2O_4)_3\cdot 10H_2O + 3e^- \quad (6c)$$

$$Fe \rightleftharpoons Fe^{2+} + 2e^- \qquad E° = -0.44\ V \quad (6d)$$

$$Fe + nHC_2O_4^- \rightleftharpoons [Fe(C_2O_4)_n]^{2-2n} + nH^+ + ne^- \quad (6e)$$

Moreover, oxidation to ferric ions (Eq. (7a)), evolution of oxygen (Eq. (7b)), oxidation of oxalate to form carbonic acid or carbon dioxide (Eq. (7c)) may take place on the anode [57], especially at the highly noble anode potential (>0.8 V) during electrolysis in a mixture of sulfuric and oxalic acid (Fig. 5S). Hydrogen evolution (Eq. (7d)) takes place on the cathode.

$$Fe^{2+} \rightleftharpoons Fe^{3+} + e^- \qquad E° = 0.77\ V \quad (7a)$$

$$2H_2O \rightarrow O_2 + 4H^+ + 4e^- \qquad E° = 1.23\ V \quad (7b)$$

$$HC_2O_4^- \rightleftharpoons H^+ + 2CO_2 + 2e^- \quad (7c)$$

$$2H^+ + 2e^- \rightleftharpoons H_2 \quad (7d)$$

Due to reaction 7d, an increase in the solution pH was observed during electro-leaching (see Fig. 2S in supplementary material), because in the beginning protons were reduced on the cathode causing hydrogen evolution. For 0.1 M H_2SO_4, increase was more pronounced and after an hour pH reached 3.8 and a reddish insoluble sediment containing most likely iron hydroxides and oxides was formed. Addition of 0.05 M $H_2C_2O_4$ led to a less significant pH rise as the oxalic acid acts as a buffering agent thus keeping pH more or less constant.

According to the measured polarization curves shown in Fig. 6, the only process is metals dissolution up to around −0.5 V(SHE) followed by nearly constant current density and eventually evolution of oxygen (not shown in Fig. 6). However, there is no drop in current density that is typical for passivation cases. For sulfuric acid leaching (Fig. 6*a*), both the initial slopes and the plateau current density increase with increasing acid concentration, probably because of the conductivity effect. As seen in Fig. 6*b*, the presence of oxalate as a significant effect on the slopes at the lowest sulfuric acid concentration. This may be explained by the formation of an oxalate layer (Figure 7, *h*), which slows down the mechanical degradation of the surface thus allowing maintenance of the high surface area.

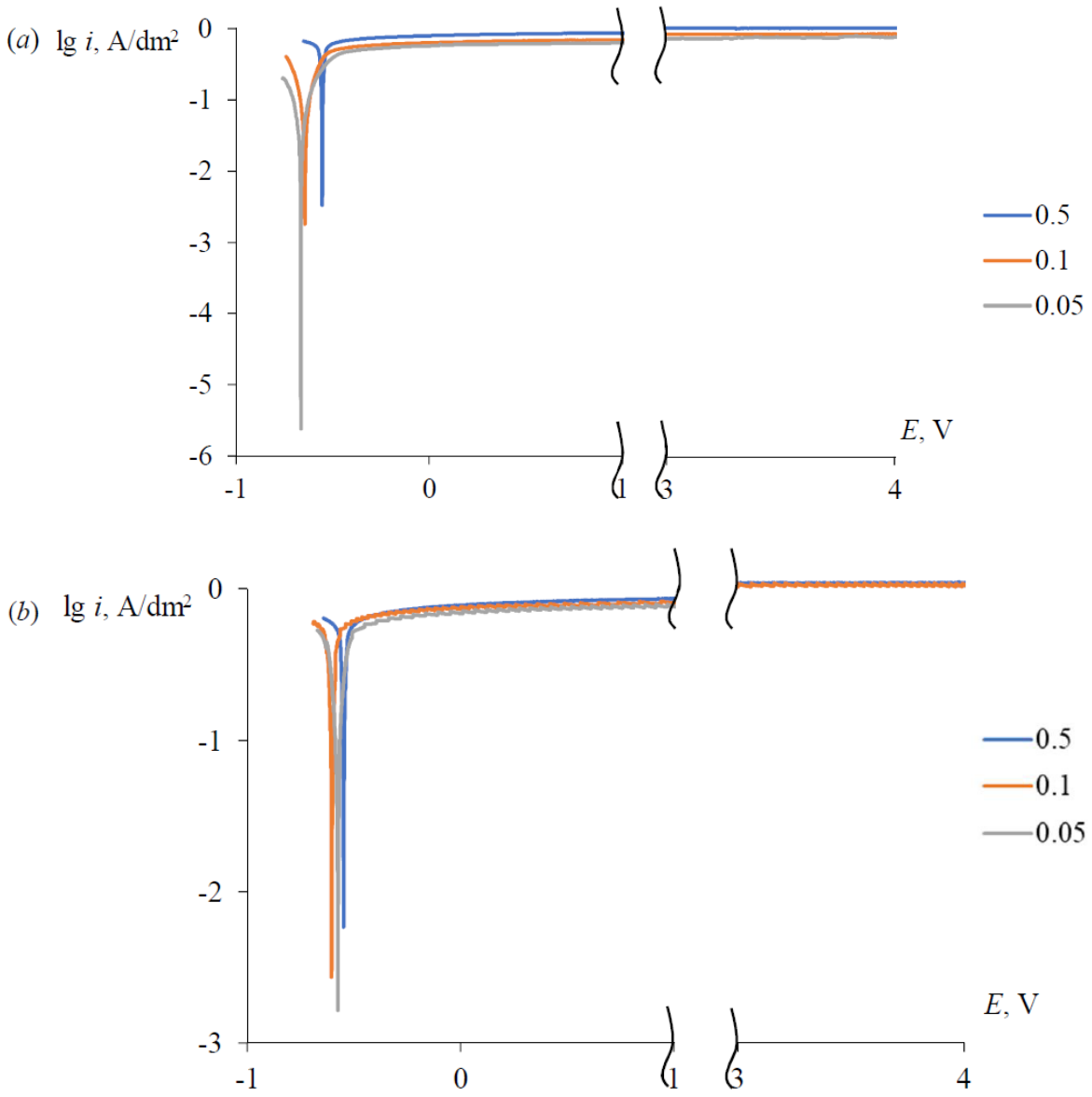

Figure 6. Linear polarization curves of the polished NdFeB magnet in sulfuric acid solutions (*a*) without oxalic acid and (*b*) in presence 0.05 M $H_2C_2O_4$.

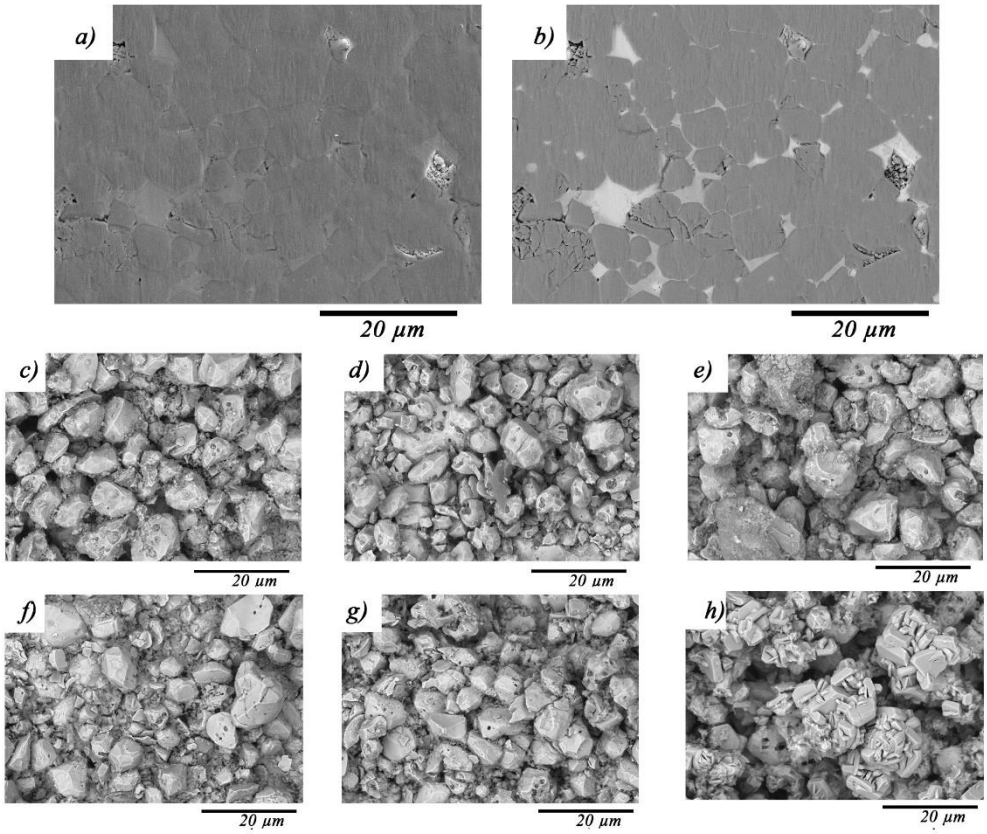

Figure 7. Microstructure of initial FeNdB magnet SE-SEM (*a*) and BSE-SEM (*b*) image of the surface after leaching in mixture 0.1 M H_2SO_4 (*c*-*e*) and in 0.1 M H_2SO_4+0.05M $H_2C_2O_4$ (*f*-*h*): chemical leaching (*a*, *f*), electrochemical at current density, A/dm^2: 10 (*d*, *g*), 20 (*e*, *h*)

3.3 Electro-leaching of powdered magnet

Electro-leaching of crushed magnet in a basket was studied in order to further improve the leaching efficiency and to make the process practically more feasible. Fe and REEs leaching from the powdered spent NdFeB magnet at different cell voltages is presented in Fig. 8. It is clear, that leaching was effective up to 30 minutes and then a plateau was reached, and leaching was completed. Significant increase of cell voltage during electrolysis was observed (Fig. 6S in supplementary material) that could be explained by decreasing surface area during the dissolution. However, the voltage increase could be eliminated by adding fresh magnet waste powder into the basket during the leaching process.

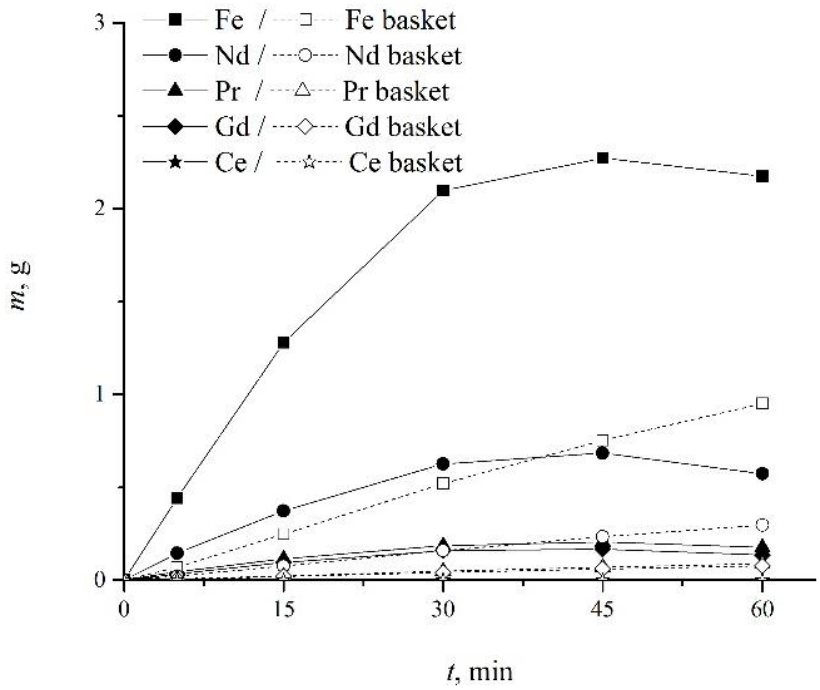

Figure 8. Comparison of iron and REEs leaching from NdFeB magnet waste powder in a basket and with plate.

3.4 Leaching mechanism of the NdFeB magnet

Based on the obtained data on chemical and electrochemical leaching, following mechanism of dissolution can be proposed (Fig. 9). Due to the heterogeneous structure of NdFeB alloy, fast and preferential leaching takes place at the less noble Nd-rich phases (Figure 7) located around the Fe-rich $Nd_2Fe_{14}B$ grains (ϕ-phase). This is reasonable considering the fact that the rare earth elements represent some of the most active metals; their standard electrode potentials range from −2.2 to −2.5 V. As a result, whole grains of the ϕ-phase finally break off from the surface (Fig. 9). Schultz et al. [16] suggested a composition-based mechanism and presence of two different intergranular phases: η-phase is B-rich and n-phase is Nd-rich phase (Nd_4Fe). Established by EDX analysis in this work; mole ratio of Nd and Fe in the intergranular phase shows higher amount of Fe.

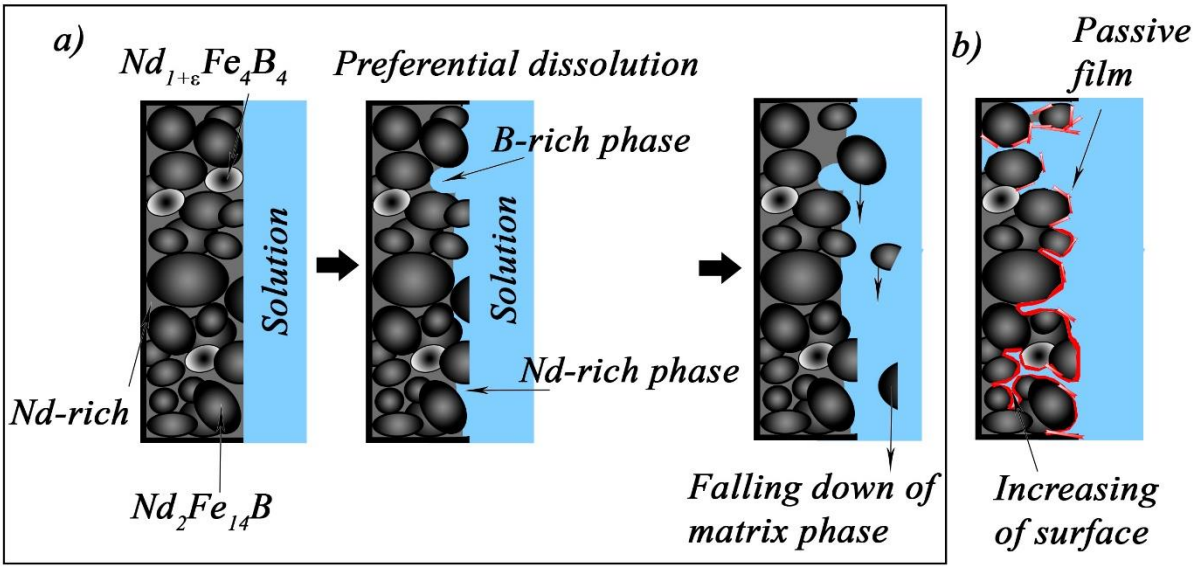

Figure 9. Schematic illustration of leaching process on the surface of spent NdFeB magnet in *a)* H_2SO_4, *b)* mixture of H_2SO_4 and $H_2C_2O_4$

3.5 Characterization of the cathodic sediment

Micrographs and EDX results of the cathode coatings are presented in Fig. 10 and Table 4. The most compact coating with strong adhesion was obtained from an electrolyte that contained only H_2SO_4 at the current density of 10 A/dm^2 (Fig. 10*a*). The cracks seen are typical for iron deposits. The coating formed in the mixture of 0.1 M H_2SO_4 and 0.05 M $H_2C_2O_4$ at current density of 20 A/dm^2 (Fig. 10*d*) showed cornflower-like structures. Increasing the current density in 0.1 M H_2SO_4 led to a creation of dendrites that could be easily removed from the cathode surface.

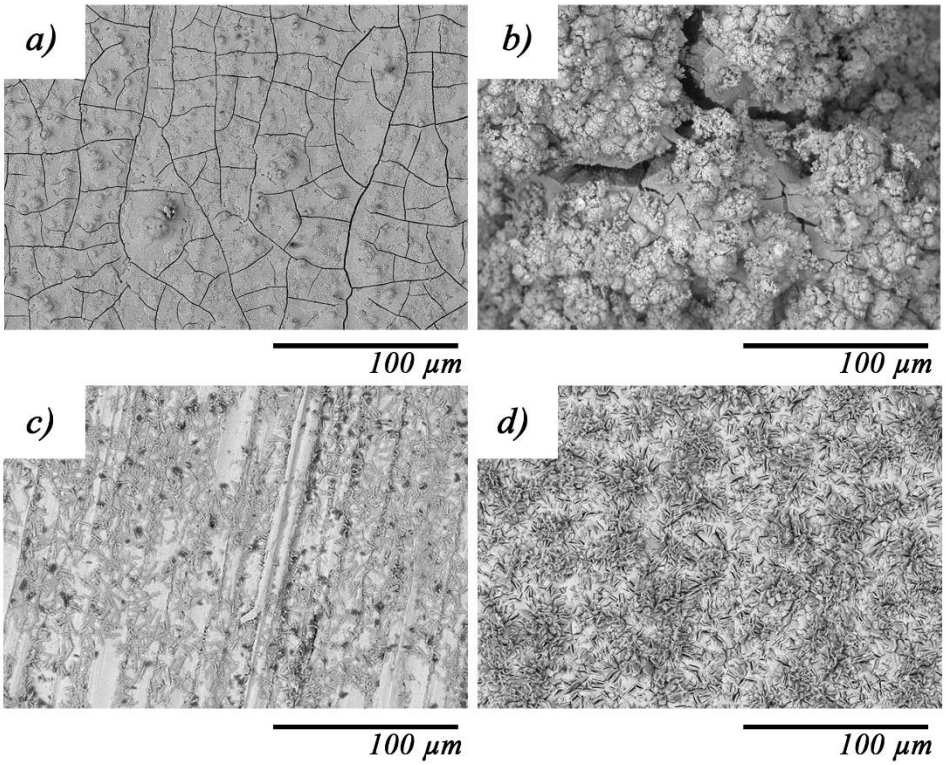

Figure 10. Micrographs of the cathode surface after 1 hour electrolysis (*a, b*) in 0.1 M H_2SO_4, (*c, d*) in mixture 0.1 M H_2SO_4 and 0.05 M $H_2C_2O_4$ at current density (*a, c*) 10 A/dm^2 and (*b, d*) 20 A/dm^2.

As mentioned above, REEs have strong negative reduction potentials and cannot be reduced in aqueous solutions, but EDX data indicated substantial amount of these elements in the cathode sediments. This most probably stem from mechanical inclusion of the REE precipitates in the growing deposit layer. Large amount of oxygen shows that oxides of Nd and Pr were included in the iron coatings and in the presence of $H_2C_2O_4$, oxalates of these metals seem to be included in the coatings. Besides, we assumed that formed oxalic complexes of REEs could be deposited directly on cathode as reduction from complexes could takes place at much more noble potentials as from individual ions. Another possibility of inclusion at high current density in 0.1 M H_2SO_4 could be caused by increasing of pH (Fig. 2S) due to cathodic reaction that leads to precipitation of basic Nd sulfate. The basic salts of Nd and $Nd(OH)_3$ could be included in cathode sediment. At the current density of 10 A/dm^2, only a small amount of coating was obtained from the mixture of 0.1 M H_2SO_4 and 0.05 M $H_2C_2O_4$.

Table 4. EDX analysis of the cathodic deposit (the values are in wt-%)

	0.1 M H_2SO_4	0.1 M H_2SO_4 and 0.05 M $H_2C_2O_4$

	10 A/dm^2	20 A/dm^2	10 A/dm^2	20 A/dm^2
C	2.9	3.9	12.8	11.7
O	17	28.3	19	24.1
Al	0.5	0.3	–	–
S	1.4	0.9	–	–
Fe	62	44.7	5.3	30.3
Ce	–	4	–	–
Pr	2.9	3.2	2.7	6.4
Nd	13.2	14.7	10.6	27.4

3.7 Energy consumption

The cell voltages measured during the electrolysis at different conditions are presented in Fig. 7S in supplementary material and the calculated energy consumptions listed in Table 5. At the current density of 10 A/dm^2, insignificant increase in cell voltage was observed. Increasing the current density up to 20 A/dm^2 led to voltage values of 10 V in sulfuric acid and mixture of sulfuric and oxalic acid. Obviously, addition of oxalate at lower current densities allows lower cell voltage, which respectively decreases the energy consumption. Decreasing of voltage is related to the blocking of the surface, which inhibits the mechanical degradation of the matrix. This on its behalf led to the growth of the electrode surface area, which decreases the voltage.

Table 5. Energy consumption (kWh/kg magnet) of electro-leaching.

i, A/dm^2	0.1 M H_2SO_4	0.1 M H_2SO_4 + 0.05 M $H_2C_2O_4$
10	2.9	0.7
20	10.1	10.0

4. Conclusions

In this study we investigated the leaching process of spent NdFeB magnet via chemical and electrochemical methods for the recovery of REEs. XRD and SEM/EDX analyses revealed the presence of $Nd_2Fe_{14}B$ micrometer-sized ferromagnetic granules surrounded by Nd-rich phases. Local Volta potential differences as high as 500 mV within the microstructure suggests preferential selective leaching of the Nd-rich phase and this was proven by chemical and electrochemical leaching experiments with 0.05 – 0.5 M H_2SO_4. The leaching rate strongly

depends on the acid concentration and current density. The positive effect of applied voltage was significant especially at low acid concentrations thus making the leaching process more environmentally friendly. Addition of oxalic acid in the leaching solution further reduces the energy consumption and at the same time improves recovery of REEs as solid oxalates. Some of the REEs were also found in the cathodic deposits. Therefore, optimizing the leaching conditions is highly important in order to make the new process viable in large-scale applications.

As a step towards realistic separation process, electro-leaching of powdered NdFeB magnet was studied using a 3D-printed titanium basket as the holder. The obtained results verify the efficiency observed with polished magnets and give basis for further development . The present paper indicates a clear potential for the electrochemical leaching methods to recover REEs from the magnet waste.

Acknowledgments

Financial support of this work from European Regional Development Fund 2014−2020 (project code A74334) is gratefully acknowledged. The authors are grateful to Dr. Liisa Puro and Dr. Toni Väkiparta for their kind support during this project and help in ICP and SEM/EDX measurements; Antti Heikkinen for his helpful comments and assistance in mechanical polishing, and Santtu Heinilehto for his help in XRD analysis.

References

1. Hoogerstraete, T.V., Blanpain, B., Gerven, T.V., Binnemans, K., 2014. From NdFeB magnets towards the rare-earth oxides: a recycling process consuming only oxalic acid. RSC Adv. 4, 64099-64111. https://doi.org/10.1039/C4RA13787F.

2. Charles, N., Tuduri, J., Guyonnet, D., Melleton, J., Pourret, O., Rare Earth Elements in Europe and Greenland: A geological potential? An overview, 12th meeting of the Society of Geology Applied to Mineral Deposits (SGA), 201,1698-1701.

3. Mio, H., Lee, J., Nakagawa, T., Kano, J., Saito, F., 2001. Estimation of extraction rate of yttrium from fluorescent powder by ball milling. Mater. Tran. 42(11), 2460−2464. https://doi.org/10.2320/matertrans.42.2460.

4. Rabah, M.A., 2008. Recyclables recovery of europium and yttrium metals and some salts from spent fluorescent lamps. J. Waste Manag. 28, 318–325. https://doi.org/10.1016/j.wasman.2007.02.006.

5. Fidler, J., Schrefl, T., Hoefinger, S., Hajduga, M., 2004. Recent developments in hard magnetic bulk materials. J. Phys.: Condens. Matter. 16, S455–S470. https://doi.org/10.1002/chin.200427200

6. Lyman, J.W., Palmer, G.R., 1993.Recycling of rare earths and iron from NdFeB magnet scrap high temperature materials and processes. 11(1), 175-187. https://doi.org/10.1515/HTMP.1993.11.1-4.175.

7. Handbook of modern sensors: physics, designs, and applications Fraden, J., 2010, Springer-Verlag New York, XV, P. 663. https://doi.org/10.1007/978-1-4419-6466-3.

8. Fidler, J., Knoch, K. G., Kronmüller, H., Schneider, G., 1989. Analytical TEM study of Al-doped, "two-phase" Nd-Fe-B sintered magnets. J. Mater. Res., 4(4), 806−814. https://doi.org/10.1557/JMR.1989.0806.

9. Knoch, K.G., Schneider, G., Fidler, J., Henig, E.-Th., Kronmüller, H., 1989. A1-doped Nd-Fe-B permanent magnets: wetting and microstructural investigations. IEEE transactions on magnetics. 25(5), 3426−3428. https://doi.org/10.1109/20.42323.

10. Bernardi, J., Fidler, J., Seeger, M., Kronmüller, H., 1993. Preparation and TEM-study of sintered $Nd_{18}Fe_{74}B_6Ga_1Nb_1$. magnets. IEEE transactions on magnetics. 29, (6), 2773−2775. https://doi.org/10.1109/20.281024.

11. Fidler, J., Bernardi, J., 1991. Transmission electron microscope characterization of cast and hotworked RFe B:Cu(R=Nd,Pr) permanent magnets, J.Appl. Phys. 70, 6456−6458. https://doi.org/10.1063/1.349929.

12. Chen, Z., Xie, F., Shi, Z., Wang, L., Fu, H., 1991. Effects of grain size, Cu addition, and Nd substitution for Pr on intrinsic coercivity in cast–hot-pressed Pr-Fe-B magnets J. Appl. Phys. 70, 2868−2870. https://doi.org/10.1063/1.349351

13. Kirchner, A., Thomas, J., Gutfleisch, O., Hinz, D., Müller, K.-H., Schultz, L.,2004. HRTEM studies of grain boundaries in die-upset Nd–Fe–Co–Ga–B magnets. J. Alloy. Compd 365, 286–290. https://doi.org/10.1016/S0925-8388(03)00661-3.

14. Warren, G.W., Chang, K.E., Ma, B.M., Bounds C.O., 1993. Corrosion behavior of NdFeB with Co and V additions. J. Appl. Phys. 73, 6479−6481. https://doi.org/10.1063/1.352586.

15. Yan, A., Song, X., Wang, X., 1997. Magnetic and microstructural properties of sintered FeNdB-based magnets with W, Mo and Nb additions. J. Alloy. Compd. 257, 273−277. https://doi.org/10.1016/S0925-8388(97)00003-0.

16. Schultz, L., El-Aziz, A.M., Barkleit, G., Mummert, K., 1999. Corrosion behaviour of Nd–Fe–B permanent magnetic alloys Mater. Sci. Eng. A267, 307–313. https://doi.org/10.1016/S0921-5093(99)00107-0.

17. Mao, S., Yang, H., Song, Z., Li, J., Ying, H., Sun, K., 2011. Corrosion behaviour of sintered NdFeB deposited with an aluminium coating. Corros. Sci. 53, 1887–1894. https://doi.org/10.1016/j.corsci.2011.02.006.

18. Lorenz, T., Bertau, M., 2019. Recycling of rare earth elements from FeNdB-Magnets via solid-state chlorination. J. Clean. Prod. 215, 131−143. https://doi.org/10.1016/j.jclepro.2019.01.051.

19. Walton, A., Yi, H., Rowson, N.A., Speight, J.D., Mann, V.S.J., Sheridan, R.S., Bradshaw, A., Harris, I.R., Williams, A.J., 2015. The use of hydrogen to separate and recycle neodymium–iron–boron-type magnets from electronic waste J. Clean. Prod. 104, 236−241. https://doi.org/10.1016/j.jclepro.2015.05.033.

20. Ni'am, A.C., Wang, Y.-F., Chen, S.-W., You, S.-J., 2019. Recovery of rare earth elements from waste permanent magnet (WPMs) via selective leaching using the Taguchi method. J. Taiwan Inst. Chem. E. 97, 137−145

21. Gergoric, M., Ravaux, C., Steenari, B.-M., Espegren, F., Retegan, T., 2018. Leaching and recovery of rare-earth elements from neodymium magnet waste using organic acids metals. 8, 721. https://doi.org/10.3390/met8090721.

22. Avdibegovića, D., Yagmurlub, B., Dittrich, C., Regadío, M., Friedrich, B., Binnemans, K., 2018. Combined multi-step precipitation and supported ionic liquid phase chromatography for the recovery of rare earths from leach solutions of bauxite residues. Hydrometallurgy. 180, 229–235. https://doi.org/10.1016/j.hydromet.2018.07.023.

23. Rivera, R.M., Xakalashe, B., Ounoughene, G., Binnemans, K., Friedrich, B., Gerven, T.V., 2018. Recovery of rare earths from bauxite residue slag by high-pressure acid leaching 2nd International Bauxite Residue Valorisation and Best Practices Conference | Athens | 7-10/05/2018 | 409−415.

24. Itakura, T., Sasai, R., Itoh, H., 2006. Resource recovery from Nd–Fe–B sintered magnet by hydrothermal treatment. J. Alloy. Compd. 408–412,1382–1385. https://doi.org/10.1016/j.jallcom.2005.04.088.

25. Saito, T., Sato, H., Motegi, T., 2006. Recovery of rare earths from sludges containing rare-earth elements. J. Alloys Compd. 425, 145−147. https://doi.org/10.1016/j.jallcom.2006.01.011.

26. Sanchez-Cupido, L., Pringle, J.M., Siriwardana, A.L., Unzurrunzaga, A., Hilder, M., Forsyth, M., Pozo-Gonzalo, C., 2019. Water-facilitated electrodeposition of neodymium in a phosphonium-based ionic liquid. J. Phys. Chem. Lett. 10, 289−294. https://doi.org/10.1021/acs.jpclett.8b03203.

27. Batchu, N.K., Binnemans, K., 2018. Effect of the diluent on the solvent extraction of neodymium(III) by bis(2-ethylhexyl)phosphoric acid (D2EHPA). Hydrometallurgy. 177, 146–151. https://doi.org/10.1016/j.hydromet.2018.03.012.

28. Gujar, R.B., Ansari, S.A., Verma, P.K., Ali, S.M., Goswami, D., Yadav, A.K., Jha, S., Bhattacharyya, D., Mohapatra, P.K., 2019. Complexation of CMPO with trivalent f-cations in ionic liquid medium: Solvent extraction, spectroscopic, EXAFS and DFT studies Polyhedron. 162, 71−80. doi: https://doi.org/10.1016/j.poly.2019.01.053.

29. Batchu, N.K., Hoogerstraete, T.V., Banerjee, D., Binnemans, K., 2017. Non-aqueous solvent extraction of rare-earth nitrates from ethylene glycol to n-dodecane by Cyanex 923. Sep. Purif. Technol. 174, 544–553. https://doi.org/10.1016/j.seppur.2016.10.039.

30. Tyumentsev, M.S., Foreman, M.R.St.J., Ekberg, C., Matyskin, A.V., Retegan, T., Steenari, B.-M., 2016. The solvent extraction of rare earth elements from nitrate media with novel polyamides containing malonamide groups. Hydrometallurgy. 164, 24−30. https://doi.org/10.1016/j.hydromet.2016.05.007.

31. Xu, Y., Chumbley, L.S., Laabs, F.C., 2000. Liquid metal extraction of Nd from NdFeB magnet scrap. J. Mater. Res. 15, (11), 2296−2304. https://doi.org/10.1557/JMR.2000.0330.

32. Xu, H., Zhang, M., Yan, Y., Sun, X., Zheng, Y., Qiu, M., Liu, L., 2019. Extraction of neodymium from other fission products by co-reduction of Sn and Nd. Appl. Organomet. Chem. 33(4) e4802 https://doi.org/10.1002/aoc.4802.

33. Kobayashi, S., Kobayashi, K., Nohira, T., Hagiwara, R., Oishi, T., Konishi, H., 2011. Electrochemical Formation of Nd-Ni Alloys in Molten LiF-CaF_2-NdF_3. J. Electrochem. Soc. 158 (12), E142-E146. https://doi.org/10.1149/1.3484777.

34. Hua, Z.S., Wang, L., Wang, J., Xiao, Y.P., Yang, Y.X., Zhao, Z., Liu, M.J., 2015. Extraction of rare earth elements from NdFeB scrap by AlF_3–NaF melts. Mater Sci Technol. 31,1007–1010. https://doi.org/10.1179/1743284714Y.0000000672.

35. Jiang, J., Ozaki, T., Machida, K.I., Adachi, G.Y., 1997. Separation and recovery of rare earths via a dry chemical vapour transport based on halide gaseous complexes. J. Alloys Compd. 260, 222-235. https://doi.org/10.1016/S0925-8388(97)00176-X.

36. Auerbach, R., Bokelmann, K., Stauber, R.O , Gutfleisch, S. Schnell, S. Ratering, 2019. Critical raw materials – Advanced recycling technologies and processes: Recycling of rare

earth metals out of end of life magnets by bioleaching with various bacteria as an example of an intelligent recycling strategy Miner. Eng. 134, 104–117. https://doi.org/10.1016/j.mineng.2018.12.022.

37. Dezhi Qi, 2018. Hydrometallurgy of Rare Earths: Extraction and Separation, Elsevier, Netherlands.

38. Ambikadevi, V.R., Lalithambika, M., 2000. Effect of organic acids on ferric iron removal from iron-stained kaolinite. Appl. Clay Sci. 16(3), 133−145. https://doi.org/10.1016/S0169-1317(99)00038-1.

39. Venkatesan, P., Hoogerstraete, T.V., Sun, Z., Binnemans, K., Sietsma, J., Yang, Y., 2018. Selective extraction of rare-earth elements from NdFeB magnets by a room-temperature electrolysis pretreatment step. ACS Sustain. Chem. Eng., 6 (7), 9375−9382. https://doi.org/10.1021/acssuschemeng.8b01707.

40. Venkatesan, P., Hoogerstraete, T.V., Hennebel, T., Binnemans, K., Sietsma, J., Yang, Y., 2018. Selective electrochemical extraction of REEs from NdFeB magnet waste at room temperature. Green Chem. 20, 1065−1073. https://doi.org/10.1039/C7GC03296J

41. P. Venkatesan, 2019. Electrochemical recycling of rare earth elements from NdFeB magnet waste, Delft University of Technology..Institutional Repository, ISBN. 978-94-6366-122-5.

42. Bockris, John O'M., Reddy, Amulya K.N., Gamboa-Aldeco, Maria E. Publisher, 2000. Modern Electrochemistry 2A Fundamentals of Electrodics, Springer US.

43. Haccuria, E., Ning, P., Cao, H., Venkatesan, P., Jin, W., Yang, Y., Sun, Z., 2017. Effective treatment for electronic waste - Selective recovery of copper by combining electrochemical dissolution and deposition. J. Clean Prod. 152, 150−156. https://doi.org/10.1016/j.jclepro.2017.03.112.

44. Pletcher, D., Walsh, F.C., 1993. Industrial Electrochemistry, Springer, Netherlands.

45. Gilbert, J.R.B., Roberts, G.M., 1982. Titanium Basket Anodes for Metal Refining and Winning. In: Williams J.C., Belov A.F. (eds) Titanium and Titanium Alloys. Springer, Boston, MA pp 2283-2290. https://doi.org/10.1007/978-1-4757-1758-7_63

46. Venkatesan, P., Sun, Z., Sietsma, J., Yang, Y., 2018. An environmentally friendly electro-oxidative approach to recover valuable elements from NdFeB magnet waste. Sep. Purif. Technol. 191, 384−391. https://doi.org/10.1016/j.seppur.2017.09.053.

47. Bala, H., Szymura, S., Pawłowska, G., Rabinovich, Y.M., 1993. Effect of impurities on the corrosion behaviour of neodymium. J. Appl. Electrochem. 23, 1017−1024. https://doi.org/10.1007/bf00266123.

48. Yu, L.Q., Wen, Y.H., Yan, M., 2004. Effects of Dy and Nb on the magnetic properties and corrosion resistance of sintered NdFeB. J. Magn. Magn. Mater. 283, 353–356. https://doi.org/10.1016/j.jmmm.2004.06.006.

49. Coy, A.E., Viejo, F., Skeldon, P., Thompson, G.E., 2010. Susceptibility of rare-earth-magnesium alloys to micro-galvanic corrosion. Corros. Sci. 52, 3896–3906. https://doi.org/10.1016/j.corsci.2010.08.006.

50. Efaw, C.M., Da Silva, T., Davis, P.H., Li, L., Graugnard, E., Hurley, M.F., 2019. Toward improving ambient Volta potential measurements with SKPFM for corrosion studies. J. Electrochem. Soc., 166 (11) C3018-C3027. https://doi.org/10.1149/2.0041911jes.

51. Dobryden, I., Touati, B., Gassoumi, A., Vomiero, A., Kamoun, N., Almqvist, N., 2017. Morphological and electrical characterization of Cu-doped PbS thin films with AFM. Adv. Mater. Lett. 8 (11), 1029−1037. https://doi.org/10.5185/amlett.2017.1545.

52. Kharitonov, D.S., Ornek, C. Claesson, P.M., Sommertune, J., Zharskii, I.M., Kurilo, I.I., Pan, J., 2018. Corrosion inhibition of aluminum alloy AA6063-T5 by vanadates: microstructure characterization and corrosion analysis. J. Electrochem. Soc., 165 (3) C116−C126. https://doi.org/10.1149/2.0341803jes.

53. Baumgartner, E., Blesa, M.A., Marinovich, H., Maroto, A.J.G., 1983. Heterogeneous electron transfer as a pathway in the dissolution of magnetite in oxaic acid solutions. Inorg. Chem., 22, 2224–2226. https://doi.org/10.1021/ic00158a002.

54. Salmimies, R., Vehmaanperä, P., Häkkinen, A., 2016. Acidic dissolution of magnetite in mixtures of oxalic and sulfuric acid. Hydrometallurgy, 163, 91–98. https://doi.org/10.1016/j.hydromet.2016.03.011.

55. Parthasarathy, P., Bulbule, K.A., 2019. Recovery of rare earth elements from spent hard disc drive magnets- urban mining suitable for developing countries. American Journal of Engineering Research (AJER) E-ISSN: 2320-0847 p-ISSN: 2320-0936 8(1), P. 137−145 www.ajer.org Research Paper Open Access

56. Um, N., Hirato, T., 2013. Dissolution behavior of La_2O_3, Pr_2O_3, Nd_2O_3, CaO and Al_2O_3 in sulfuric acid solutions and study of cerium recovery from rare earth polishing powder waste via two-stage sulfuric acid leaching. Mater. Trans., 54 (5), 713−719. https://doi.org/10.2320/matertrans.M-M2013802.

57. Vassiliev, Yu. B., Sarghisyan, S. A., 1986. Electro-oxidation of oxalic acid. Electrochim. Acta., 31 (6), 645−655. https://doi.org/10.1016/0013-4686(86)87031-1.

Supplementary material

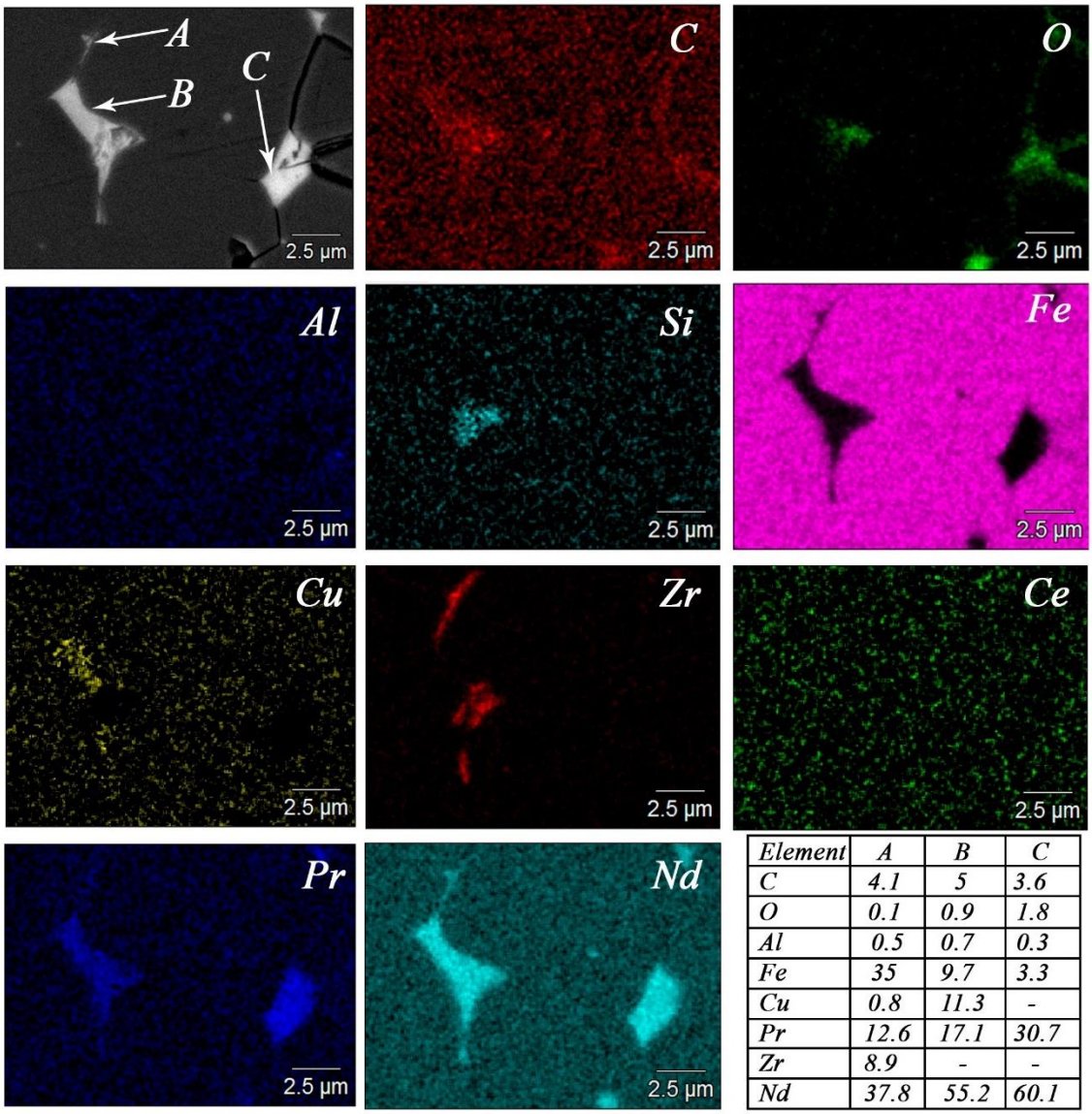

Element	A	B	C
C	4.1	5	3.6
O	0.1	0.9	1.8
Al	0.5	0.7	0.3
Fe	35	9.7	3.3
Cu	0.8	11.3	-
Pr	12.6	17.1	30.7
Zr	8.9	-	-
Nd	37.8	55.2	60.1

Figure 1S. High-resolution EDX mapping of Nd-rich phases showing different chemical composition.

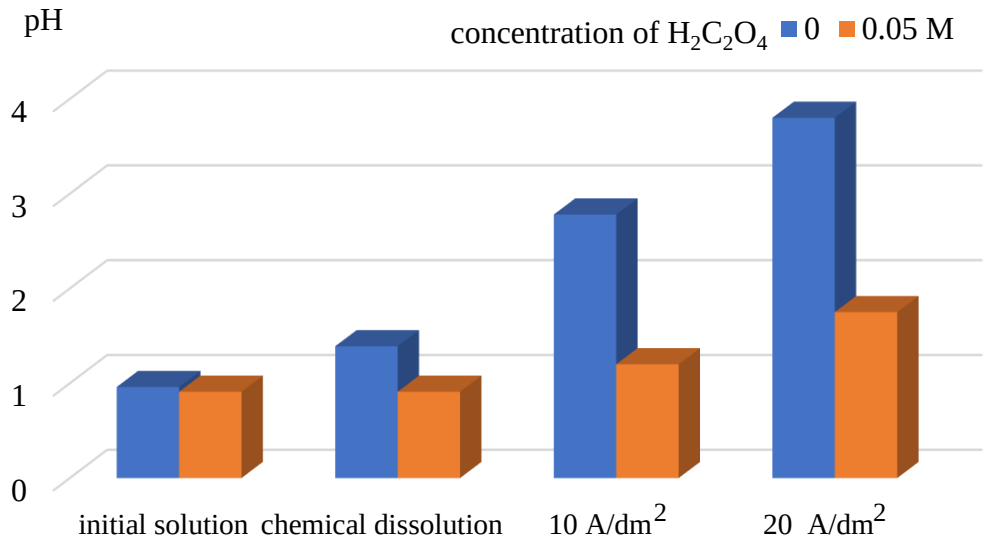

Fig. 2S. Initial pH and after 1 hour of chemical and electrochemical leaching

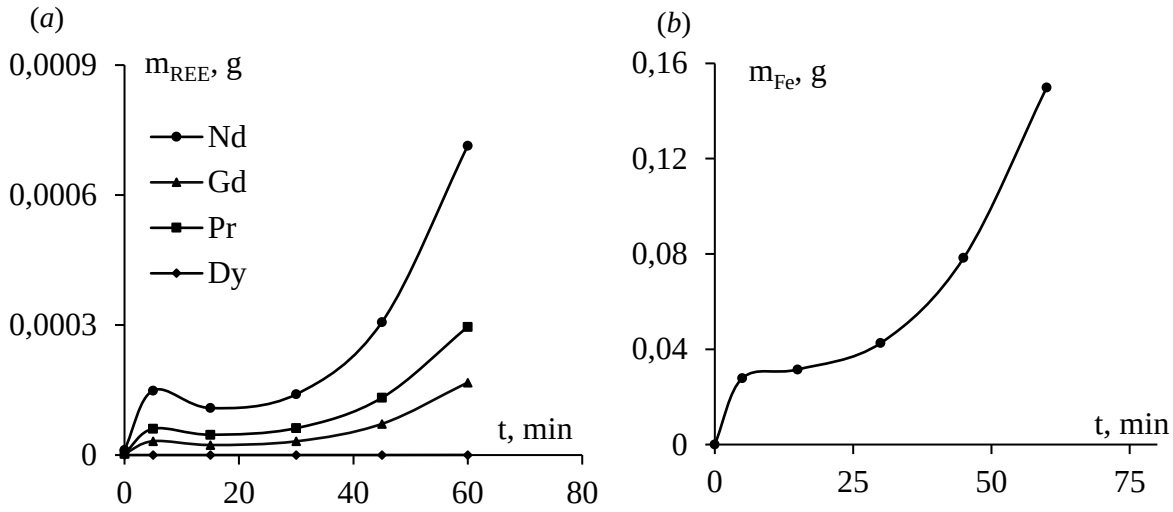

Fig. 3S. Chemical leaching of REEs (*a*) and Fe (*b*) from NdFeB magnet waste in 0.1 M H_2SO_4 + 0.1 M $H_2C_2O_4$.

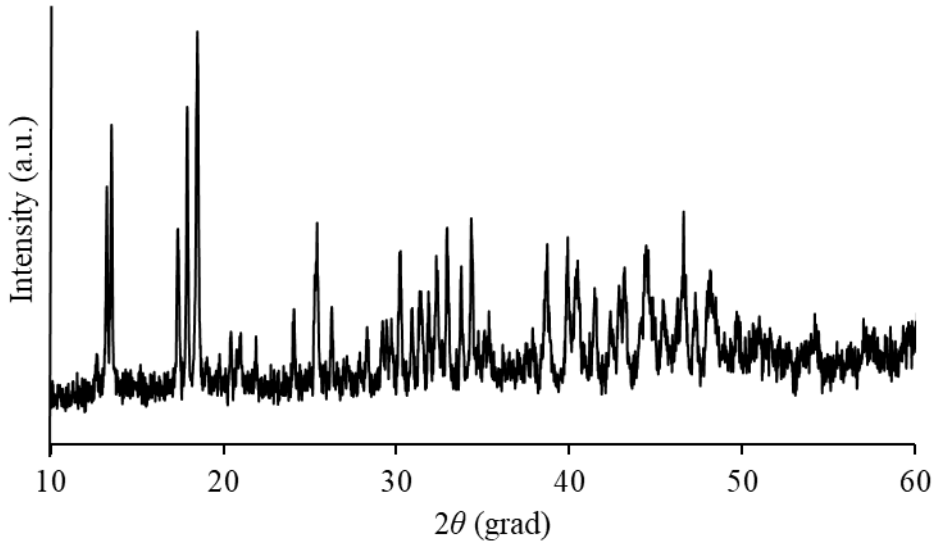

Figure 4S. X-Ray diffraction spectra of powder after electrolysis in the mixture of H_2SO_4 and $H_2C_2O_4$

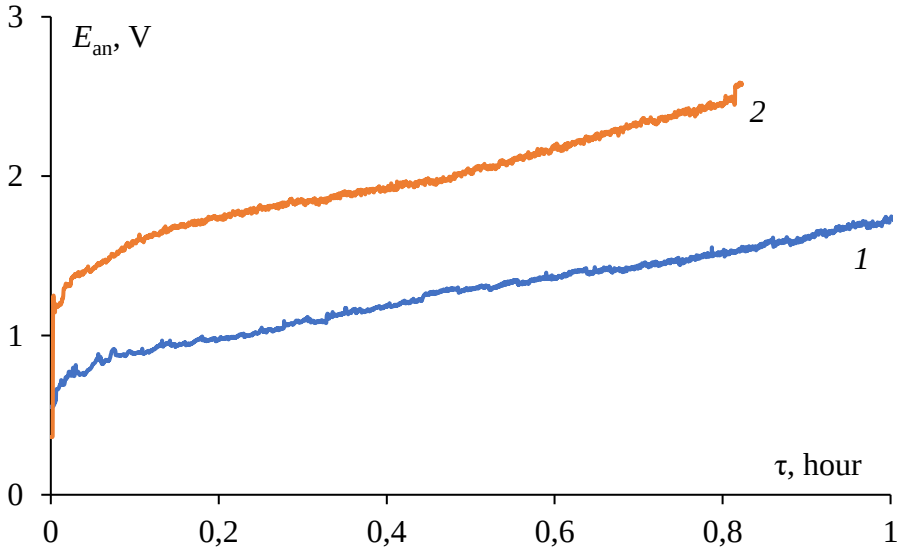

Fig. 5S. Anode potential (NdFeB magnet) during electrolysis in 0.1 M H_2SO_4 and 0.05 M $H_2C_2O_4$ at current density, A/dm^2: 1 – 10, 2 – 20.

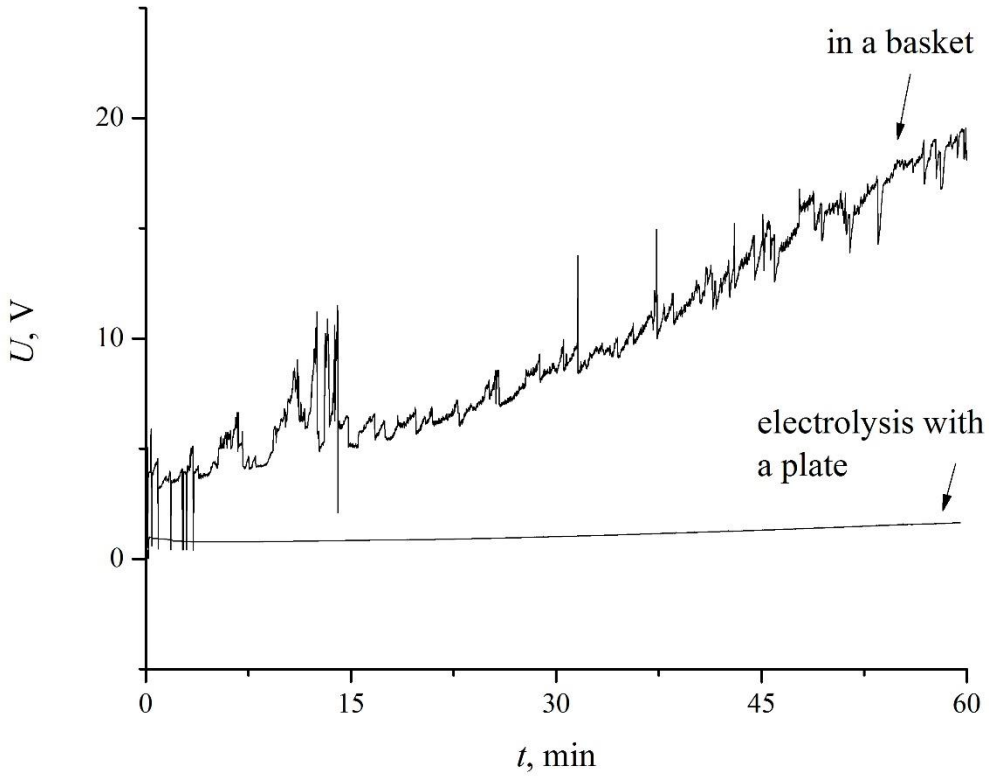

Fig 6S. Voltage on a cell in 0.5 M H_2SO_4. Stirring rate 400 rpm, T = 23 °C, i = 10 A/dm^2

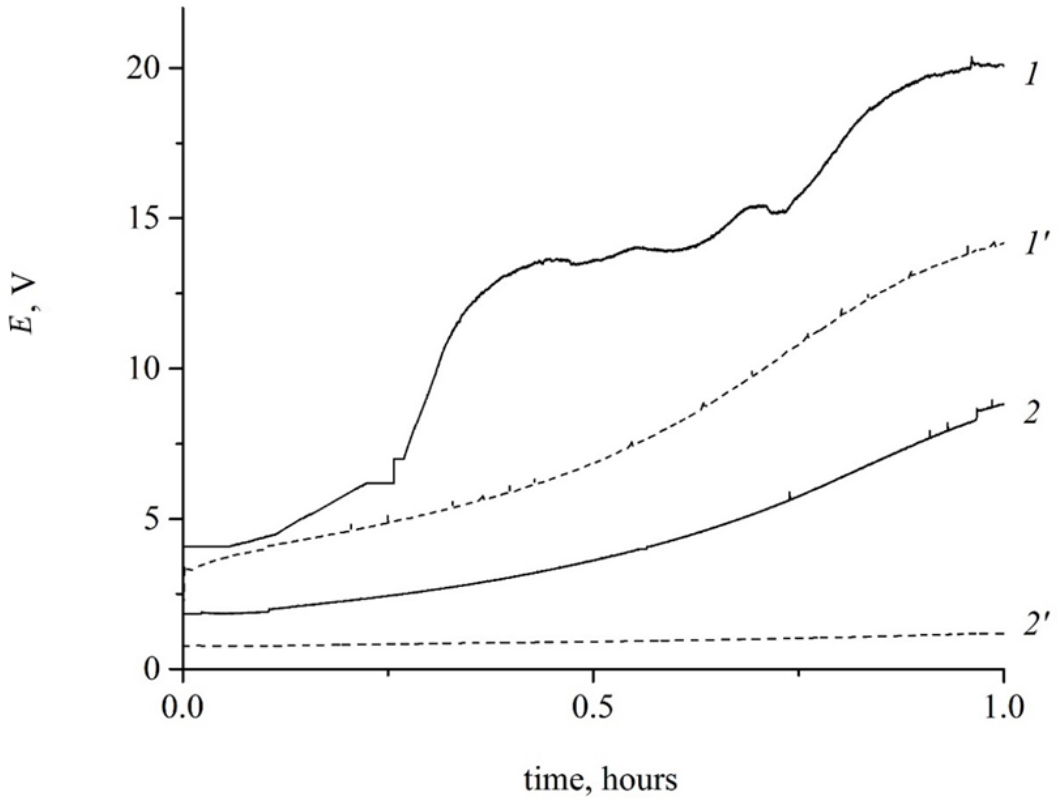

Fig. 7S. Cell voltage during electrolysis: (*1*, *2*) 0.1 M H_2SO_4, (*1*', *2*') 0.1 M H_2SO_4 + 0.05 M $H_2C_2O_4$; current density (2, 2') 10 A/dm^2 and (1, 1') 20 A/dm^2.